HiSST: International Conference on
High-Speed Vehicle Science Technology
26–29 November 2018, Moscow, Russia

Heterophase materials in $ZrSi_2$-ZrB_2-$MoSi_2$ system: synthesis, kinetics and mechanisms of high-temperature oxidation

Astapov A.N.[1], Levashov E.A.[2], Lifanov I.P.[1], Pogozhev Yu.S.[2], Potanin A.Yu.[2], Prokofiev M.V.[1], Rabinskiy L.N.[1]

[1] Moscow Aviation Institute (National Research University), 125993, Russia, Moscow, Volokolamskoe shosse, 4
[2] National University of Science and Technology «MISIS», 119049, Russia, Moscow, Leninsky prospect, 4

Abstract

This work presents the results of studying the kinetics and mechanism of high-temperature oxidation of compact heterophase ceramics in the $ZrSi_2$-$MoSi_2$-ZrB_2 system at temperatures of 1400 and 1650°C for 10 and 5 hours, respectively. Ceramics was obtained by hot pressing of composite powders made by the method of self-propagating high-temperature synthesis according to the scheme of magnesium thermal reduction. The kinetics of oxidation is described by a power law, which indicates a significant influence of evolutionary changes in the structure of the formed oxide films on the course of the process. The oxidation mechanism at 1400°C includes the formation of a two-layer structure consisting of a continuous silicate film, the outer part of which is saturated with magnesium, and a sublayer based on the $ZrSiO_4$ phase with a scheelite structure encapsulating ZrB_2 and $MoSi_2$ grains. The mechanism of oxidation at 1650°C includes the formation of a multilayer structure of a heterogeneous oxide film, the partial dissociation of the $ZrSiO_4$ phase, the formation of secondary compounds MoB and Mo_5Si_3. The effect of the $ZrSi_2$, $MoSi_2$ and ZrB_2 phases on the structural-morphological features of the forming oxide films and the effectiveness of their protective action is shown. In the $ZrSi_2$-$ZrSiO_4$ system above 1620°C, under conditions of lack or absence of oxygen, silicon is being recovered with simultaneous oxidation of zirconium to ZrO_2.

Keywords: *heterophase ceramics, self-propagating high-temperature synthesis, oxidation, kinetics, mechanism.*

Nomenclature

EDS – energy dispersive spectrometer
HP – hot pressing
m-ZrO_2 – monoclinic zirconium dioxide
SEM – scanning electron microscope
SHS – self-propagating high-temperature synthesis
t-ZrO_2 – tetragonal zirconium dioxide
XRD – X-ray diffraction analysis

1. Introduction

The need for new materials is one of the key problems arising in the development of thermal protection systems for airframes and flow paths of propulsion systems of atmospheric high-speed aircraft and reusable aerospace vehicles [1-4]. Ultra-high-temperature ceramics based on ultra-high-melting transition metal borides of Zr(Hf)B_2-SiC [3, 4], Zr(Hf)B_2-SiC-$MeSi_2$ [5-8], Zr(Hf)B_2-$MeSi_2$ [9-12] systems and others, where Me is Mo, Zr, Ta, W are promising for structural applications. In this work, the system chosen for research is the $ZrSi_2$-$MoSi_2$-ZrB_2 system based on the relatively low melting phase $ZrSi_2$ (T_m = 1620°C) in comparison with $MoSi_2$ (T_m = 2020°C) and ZrB_2 (T_m = 3245°C). The interest in these materials is caused by the possibility of their use in slip-firing technologies for modifying matrix of carbon-containing composites and for obtaining protective coatings. This is due to

their ability to form during the heat treatment a significant amount of the liquid phase, necessary for impregnation of the matrix of composites and sintering of the applied powder layers into compact coatings. From these positions, materials based on $Zr(Hf)B_2$ are unsuitable for application.

The aim of the work was to study the kinetics and mechanism of oxidation of ceramics in the $ZrSi_2$-$MoSi_2$-ZrB_2 system at temperatures of 1400 and 1650°C to determine the protective ability of materials and to evaluate the prospects for their further use as heat-resistant compositions.

2. Materials and Investigation Methods

$ZrSi_2$-$MoSi_2$-ZrB_2 composite powders were obtained by self-propagating high-temperature synthesis (SHS) including the magnesiothermal recovery stage [13]. Zirconium oxide (ZrO_2) powders, (SiO_2) silicon and molybdenum (MoO_3) of AR grade and boric anhydride (B_2O_3) including base material not less than 99 % were used as the starting components for sample preparation. MPF-3 magnesium powder (Mg) is a reducing agent including 98.5-99.5 % of active component. The preparation of reactor feed (furnace-charge) was carried out in a ball mill with tight-head drums and milling bodies in the form of cylinders of hard metal alloy WC-6 % Co. The ratio of the furnace-charge masses and milling bodies was 1:6. The experimental compositions of the charge were selected to provide after the reduction the varying of concentrations of Zr, Si, Mo, B in the intervals of mass. %: 42.3-66.2; 20.7-40.5; 4.2-14.9 and 2.1-9.2, respectively. Methods of regression analysis and numeric optimization were used to increase efficiency and shorten the duration of investigations in field of searching for chemical compositions of highly refractory materials. The experimental planning matrix was composed so that the investigated concentration points were evenly distributed in the field of interest in Si-Zr-Mo-B phase diagram.

The synthesis was carried out in a universal SHS-8 reactor [14] with 8 liters volume of the reaction chamber with the excessive argon pressure of 3 MPa. The raw materials were loaded to the graphite box by free pouring and then the box was placed into the reaction chamber. To start the combustion process, a tungsten spiral was used. Product cooling was carried out in water cooled reactor tube.

The milling of synthesis products was carried out in two stages: initially coarse fraction of particle size up to 3 mm was obtained through milling in a jaw-breaker, and further milling was carried out using the ball mill. The obtained milling powders represent the designed product mixture – composite powder of the $ZrSi_2$-$MoSi_2$-ZrB_2 system with magnesium oxide and unreacted magnesium. To separate the target product, chemical (acidic) enrichment in hydrochloric acid (HCl) water solution was used with heating in a water bath up to 40-50°C for 2 h. Then, the obtained mother liquor was decanted and the separated residue of the target product was filtered and washed with water. Further powder drying was carried out in a SSHVA-2.5-200 drying stove at the temperature of ~ 100°C. Dried powder was milled in the ball mill and classified using a PE-6800. Composite powder fraction with the particle size < 63 μm was subjected to extra milling in a planetary centrifugal mill of MPP-1.

The compact specimen was received by hot-pressing (HP) of the synthesized powders in the DSP-515 SA instrument (Dr. Fritsch, Germany) in vacuum at 1200-1250°C, heating rate of 50 °C/min, pressure of 30 MPa and 10 min isobaric storage. The compacts were obtained as discs with the diameter of 50 mm and width of 5 mm. Samples for investigations were then cut as square layers with the dimensions of 10×10×5 mm using an EDM machine ARTA 200-2.

Oxidation of samples was carried out in chamber electrical furnaces with a volume of working place of 4 liters at air at temperatures of 1400 and 1650°C by thermo cycling by different schemes. For each composition, 3-4 samples were tested. The oxidation degree was evaluated by the specific weight of samples. Weighing was carried out on an analytical balance AND GR-202 with an accuracy of 10^{-4} g.

Oxidation at 1400°C was performed in a TK.4.1400.1F furnace with SiC heaters. Corundum crucibles with samples were loaded into a furnace preheated to 1400°C, then isothermal exposure was carried out for a specified time, after which the samples were cooled in air at room temperature. Weighing was performed together with crucibles up to 1 hour of total isothermal oxidation every 15 minutes, then up to 2 hours every 30 minutes, then up to 5 hours every 60 minutes, and then up to 10 hours every 150 minutes.

Oxidation at 1650°C was carried out in a Nabertherm LHT 04/17 SW furnace with $MoSi_2$ based heaters. Samples in corundum crucibles were loaded into the furnace at a chamber temperature of

20°C, then heated to 1650°C at a heating rate of 40 °C/min, isothermally kept for a specified time, cooled with the furnace to 20°C, removed from the furnace and weighed. The first two thermal cycles were performed with an isothermal holding of 30 min, the rest 60 min each. The total isothermal holding time at 1650°C was 5 h.

The phase composition was determined by X-ray diffraction analysis (XRD) on an ARL X'tra diffractometer from Thermo Scientific. Microstructural studies were performed using Hitachi S-3400N and Carl Zeiss EVO-40 scanning electron microscopes (SEM) equipped with NORAN System and X-Max Oxford Instruments X-ray energy dispersive spectrometers (EDS), respectively. The samples were manufactured on high-precision equipment from Struers. After the oxidation of the samples, carbon films 50-100 nm thick were deposited on their surface on the vacuum universal post VUP-4 to ensure the flow of electric charge transported to the dielectric surface by a scanning electron beam.

3. Results of research and discussion

3.1. The composition and structure of ceramics in the $ZrSi_2$-$MoSi_2$-ZrB_2 system

Compact samples for research were obtained from the 16 composite powder materials synthesized in the $ZrSi_2$-$MoSi_2$-ZrB_2 system with different phase ratios. According to XRD data, the main phases in the composition of the samples are $ZrSi_2$, $MoSi_2$ and ZrB_2. In addition to these compounds, zircon (zirconium orthosilicate) $ZrSiO_4$ is present in all samples. In some samples, the m-ZrO_2 phase and crystalline silicon were also detected. Table 1 selectively presents the results of X-ray diffraction, data on hydrostatic ρ_{hydr} and true ρ_{true} density, as well as the values of residual porosity P_{res} of the compact HP-samples.

Table 1. Phase composition, density and residual porosity of the original compacts

Composition	Phase composition, mass. %						ρ_{hydr}, g/cm^3	ρ_{true}, g/cm^3	P_{res}, %
	$ZrSi_2$	$MoSi_2$	ZrB_2	Si	$ZrSiO_4$	m-ZrO_2			
1	42	22	13	3	20	–	4.8	4.9	2.9
2	48	13	33	–	6	–	4.6	4.8	2.5
3	22	14	47	–	9	8	5.3	5.5	3.5

The results of structural studies (according to SEM and EDS) showed that in all samples the matrix is zirconium disilicide $ZrSi_2$. ZrB_2 particles in the form of elongated crystals of regular cut and $MoSi_2$ grains are relatively uniformly distributed inside the matrix. The inclusions corresponding to the $ZrSiO_4$ phase are located at the grain boundaries of the matrix phase. These results of microstructural studies are in good agreement with the XRD data. In addition, all samples revealed oxide inclusions that contain elements of Mg-Si-O in a ratio close to 1:1:2. In some samples, inclusions with elemental composition corresponding to pure Si are also found. The Mg-Si-O inclusions, as well as elemental silicon and $ZrSiO_4$, are distributed along the boundaries of the $ZrSi_2$ and $MoSi_2$ silicides. Since the presence of magnesium silicates was not detected by XRD, it can be assumed that this is due to their X-ray amorphous state.

3.2. Kinetics and mechanism of ceramics oxidation at 1400°C

The kinetic curves of oxidation of compacts at 1400°C are presented in Fig. 1*a* in the form of dependences of the specific weight gain per unit surface area of the samples q on the test time t. Here the experimental data are shown by the markers, and the solid curves show the results of their approximation using the power dependence $q^n = k \cdot t$, where k is the oxidation process constant; n is an indicator of a power law. The values of the parameters k, n obtained by approximation of the experimental data are presented in Table 2. The experimental data of specific weight gains q_Σ of compacts after 10 hours of isothermal exposure at 1400°C is also presented there. It can be seen that the kinetics of oxidation of samples of all compositions is described by a power law with an exponent $n > 2$, which indicates evolutionary processes in the structure of the forming oxide films. Figure 1*b* shows the time variation of the oxidation rates of the samples. It is seen that at the initial moment of oxidation, the rates are maximum, however, due to the rapid formation of heat-resistant films, their values rapidly decrease (stage I). Subsequently, the oxidation rates continue to monotonously decrease (stage II) due to the continuous inhibition of the diffusion of the reactants through the growing oxide layer and their values almost reach the plateau. The boundary between the marked stages of oxidation is rather arbitrary and does not have an unambiguous definition. As a

boundary criterion separating the indicated steps, we, by analogy with the half-life of quantum-mechanical systems, chose time $t_{1/2}$, during which the specific weight of the samples would be ½ of their total gain q_Σ for the entire oxidation time. The calculated values of these times are given in Table 2 and for clarity, marked with markers in Fig. 1*b*. Table 2 also presents the calculated values of the average oxidation rates of v_{av} of the samples at each of the indicted stages.

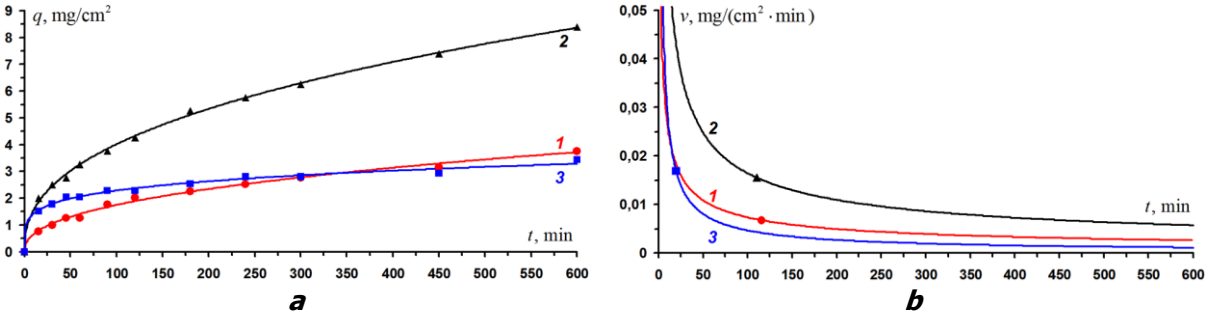

Fig. 1. Kinetic curves of oxidation of ceramic samples of compositions *1-3* at 1400°C (*a*) and the corresponding oxidation rates (*b*)

Table 2. Characteristics of the kinetics of oxidation of compacts at 1400°C and thickness (h_Σ) of the formed oxide layers after 10 hours of isothermal exposure

Composition	q_Σ, mg/cm²	*k*	*n*	$t_{1/2}$, min	v_{av}, mg/(cm²·min)		Thickness of oxide layer, μm		
					stage I	stage II	surface / Mg saturated	sublayer	h_Σ
1	3.770	0.037	2.372	115.9	0.016	$3.826 \cdot 10^{-3}$	12-17 / 6-9	14-18	30-35
2	8.393	0.3	2.445	110.2	0.038	$8.533 \cdot 10^{-3}$	8-11 / 8-11	40-45	50-55
3	3.435	0.583	4.928	19.7	0.083	$2.828 \cdot 10^{-3}$	8-12 / 5-7	45-50	55-60

Typical results of structural studies of cross sections of samples using SEM and EDS after their 10-hour oxidation at 1400°C are presented in Fig. 2 in the form of images of microstructures in secondary electrons and corresponding X-ray maps of the distribution of elements.

A common feature for all samples is the formation of a two-layer oxide film in the process of their oxidation, represented by (i) a surface layer based on SiO_2, $MgSiO_3$ and Mg_2SiO_4, and a sublayer (ii) based on $ZrSiO_4$ and ZrO_2. It is established that magnesium, initially uniformly distributed in the volume of the initial compacts, is concentrated in the surface layer (i) in the form of $MgSiO_3$ during the oxidation process. The formation of a continuous vitreous film (i) on the surface of the samples with the presence of individual dispersed $ZrSiO_4$ particles indicates the migration of a significant part of magnesium silicate and SiO_2 from the sublayer. The absence of boron oxide or borates in the composition of oxidation products on the surface indicates that phases that do not contain boron, i.e. $ZrSi_2$ and $MoSi_2$ are oxidized preferably. The composition, thickness, and morphology of the oxidation products for compacts 1-3 differ significantly (especially in the near-surface zone). Summary data on the thickness of the formed oxide layers are presented in Table 2.

According to XRD data, the main phases in the composition of the surface layers of the samples are $MgSiO_3$, Mg_2SiO_4 and SiO_2. Since the thickness of the surface layer for all samples is less than the depth of penetration of X-rays, which, according to our estimates, is 15-20 μm, the X-ray diffraction data from the surface of the samples also contains information about the phase composition of the upper part of their oxide sublayer. This is evidenced by the $ZrSiO_4$ phase recorded in all samples. After grinding the surface oxide layer to a depth of ~ 20 μm, the underlying oxide layers of the samples are represented by the $ZrSiO_4$ and m-ZrO_2 phases. It should not be excluded that X-ray amorphous silica which cannot be registered by XRD is present in the composition of oxidation products. The presence in the sublayer of composition 3 of a significant amount of the $MoSi_2$ and ZrB_2 initial phases in the absence of $ZrSi_2$ indicates preferential oxidation in the matrix phase of $ZrSi_2$.

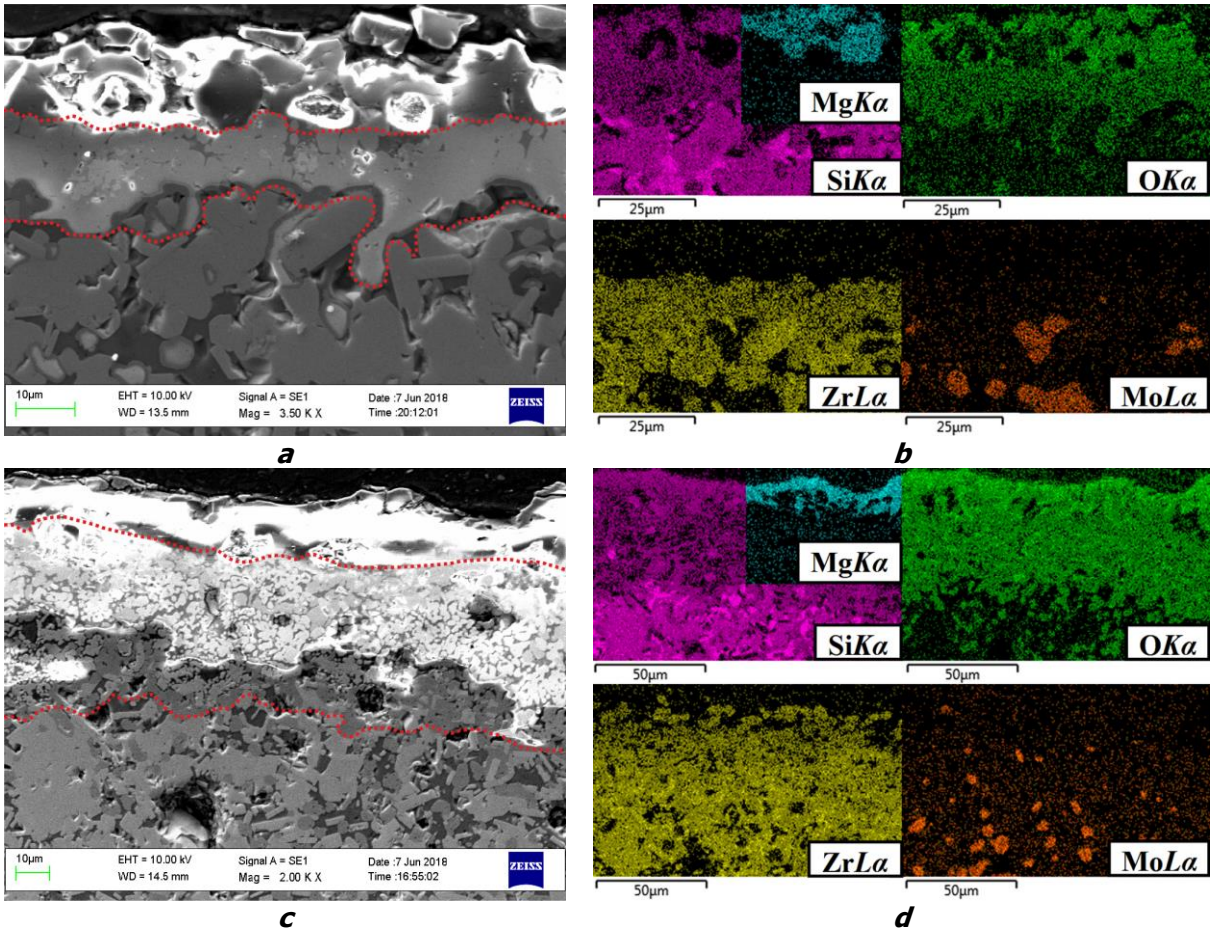

Fig. 2. Microstructure (*a*, *c*) and distribution of elements in characteristic X-rays (*b*, *d*) in samples after isothermal oxidation at 1400°C, 10 h: composition *1* - *a*, *b*; composition *2* - *c*, *d*

Analysis of the obtained results allows us to propose the following mechanism for the oxidation of ceramics of the $ZrSi_2$-$MoSi_2$-ZrB_2 system. At a temperature of 1400°C, the surface is passivated, preventing the spreading of active oxidation into the depth of compacts. Component oxidation processes are described by the reactions:

$$ZrSi_{2(s)} + 3O_{2(g)} \rightarrow ZrO_{2(s)} + 2SiO_{2(s)} \ (\Delta G_{1400°C} = -1858.4 \text{ kJ/mol}); \quad (1)$$

$$5MoSi_{2(s)} + 7O_{2(g)} \rightarrow 7SiO_{2(s)} + Mo_5Si_{3(s)} \ (\Delta G_{1400°C} = -3999.9 \text{ kJ/mol}); \quad (2)$$

$$2ZrB_{2(s)} + 5O_{2(g)} \rightarrow 2ZrO_{2(s)} + 2B_2O_{3(l)} \ (\Delta G_{1400°C} = -2740.7 \text{ kJ/mol}); \quad (3)$$

and are accompanied by the interaction of oxidation products:

$$xSiO_{2(s)} + yB_2O_{3(l)} \rightarrow xSiO_2 \cdot yB_2O_{3(s,l)} \ (\Delta G_{1400°C} < 0 \text{ kJ/mol}); \quad (4)$$

$$ZrO_{2(s)} + SiO_{2(s)} \rightarrow ZrSiO_{4(s)} \ (\Delta G_{1400°C} = -2.2 \text{ kJ/mol}). \quad (5)$$

Obviously, in terms of 1 mol of the starting materials, the oxidation of $ZrSi_2$ according to reaction (1) is more thermodynamically preferably than the oxidation of $MoSi_2$ and ZrB_2 according to reactions (2) and (3). Our studies have shown that from the kinetic point of view, the oxidation of $ZrSi_2$ in heterophase materials of the $ZrSi_2$-$MoSi_2$-ZrB_2 system occurs much faster than $MoSi_2$ and ZrB_2, as evidenced by the predominant oxidation of the samples in the $ZrSi_2$ matrix phase. One of the possible reasons is the selective oxidation of zirconium in $ZrSi_2$, leading to the formation of a heterogeneous film containing, in addition to amorphous SiO_2, a significant amount of crystalline zirconium dioxide ZrO_2 with high ionic conductivity of oxygen. The oxygen permeability of ZrO_2 contributes to the relatively rapid spread of oxidation into the depths, especially at the initial stage, until the formation of a continuous vitreous layer providing an effective barrier to the diffusion of oxygen. On the contrary, the selective oxidation of silicon in $MoSi_2$ leads to the formation of a heat-resistant SiO_2 film, enveloping the $MoSi_2$ grains and protecting them from further oxidation. ZrB_2 particles are also

susceptible to oxidation mainly at the initial stage, before the formation glass phase which encapsulates them.

The interaction of the primary oxidation products with each other, limited by the rate of diffusion mass transfer of reagents in a complex heterogeneous system, leads to the formation of: (i) a borosilicate glass phase with a single anionic matrix according to reaction (4); (ii) a new crystalline phase of $ZrSiO_4$ by reaction (5). In the present work, the distribution of boron in glass was not quantified because of the low sensitivity of the EDS to light elements, especially with a low content (in the reaction (4) $y << x$). The formation of zircon $ZrSiO_4$ is a solid-phase reaction. It should be noted that zircon has a scheelite type structure, which is characterized by a high packing density of atoms in the crystal lattice. This leads to a decrease in the diffusion of oxygen through $ZrSiO_4$ and increases the heat resistance of materials in the structure of which this phase is present or formed during operation.

In the process of oxidation, a two-layer oxide film is formed, which is represented by (i) a surface layer of silicate glass with $ZrSiO_4$ particles separately located in it and (ii) a sublayer based on $ZrSiO_4$ and ZrO_2. The main driving force for the growth of the outer vitreous layer is the transport to the surface of viscous-flowing SiO_2, which is formed mainly by reaction (1), due to the volume expansion resulting from the oxidation of $ZrSi_2$. Assuming that the oxidation products have a theoretical density, 1 unit of volume of $ZrSi_2$ gives 0.67 units of volume of t-ZrO_2 and 1.5 units of volume of SiO_2. The volume increase during oxidation compared with the initial $ZrSi_2$ phase is 117 %. The formation of borosilicate glass according to reaction (4) lowers the glass transition temperature in comparison with silica, improves viscous-flow properties and facilitates transport of the glass phase to the surface. Other possible driving forces of the upwelling of SiO_2, such as a temperature gradient and a chemical potential gradient, are unlikely: oxidation at 1400°C was carried out in isothermal conditions, and the concentration of SiO_2 in the inner part of the oxide zone is lower than in the outer.

Simultaneously with the formation of a continuous outer oxide layer, segregation of magnesium initially evenly distributed in the volume of the original compacts, occurs in its outer part, apparently due to the high diffusion rate in the structural components, which at 1400°C are in a viscous-plastic state. Magnesium segregation is associated, on the one hand, with its surface activity with respect to silicon and zirconium, characterized by a lower surface tension value. On the other hand, magnesium has a higher reactivity when interacting with oxygen than zirconium, silicon and boron, as evidenced by the comparative data of the difference in relative electronegativity values according to L. K. Pauling between oxygen and these elements. In our opinion, the formation of an outer layer of glass with a high content of magnesium metasilicate $MgSiO_3$ helps to reduce the glass transition temperature and viscosity (in comparison with silica), increases the wetting properties of the film, which generally improves the ability of the glass phase to heal defects.

3.3. Kinetics and mechanism of ceramics oxidation at 1650°C

The kinetic curves of oxidation of compacts at 1650°C are presented in Fig. 3*a* in the form of dependences of the specific weight per unit surface area of the samples q on the test time t. Fig. 3*b* shows the time variation of the oxidation rates of the samples. The values of the kinetic parameters k, n obtained by approximating the experimental data are given in Table 3 together with experimental data on specific weight gains of samples q_{30} and q_{Σ} after 30 min and 5 hours of isothermal exposure at 1650°C, respectively. It also presents the calculated values of the average oxidation rates of v_{av} of the samples at stages I and II, as well as the values of the transition times $t_{1/2}$.

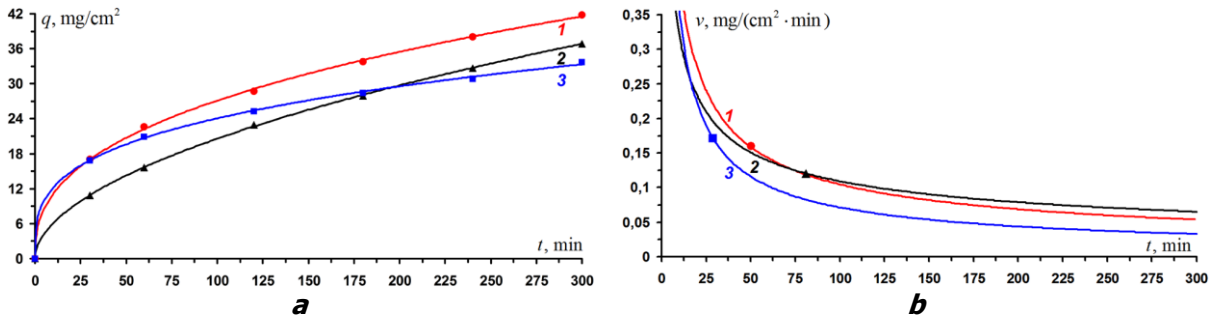

Fig. 3. Kinetic curves of oxidation of ceramic samples of compositions *1-3* at 1650°C (*a*) and the corresponding oxidation rates (*b*)

Table 3. Characteristics of the kinetics of oxidation of compacts at 1650°C after total isothermal exposure for 5 hours

Composition	q_{30}, mg/cm^2	q_{Σ}, mg/cm^2	k	n	$t_{1/2}$, min	v_{av}, mg/(cm^2·min)	
						stage I	stage II
1	19.234	41.798	49.525	2.579	50.2	0.413	0.083
2	12.892	36.861	3.008	1.887	81.1	0.227	0.084
3	18.849	33.636	468.692	3.383	28.8	0.578	0.061

Typical structures of cross sections of samples after their 5-hour oxidation are shown in Fig. 4 in the form of images of microstructures in secondary electrons, separate X-ray maps of the distribution of elements and multi-layer combined images created on the basis of the combination of electronic images and X-ray maps. The formed oxide films have a complex heterogeneous structure and a multilayer structure. Summary data on the thickness of the forming layers are presented in Table 4.

Table 4. Thickness of the formed oxide layers after isothermal exposure of compacts at 1650°C for 30 min and 5 hours

Composition	Thickness of the oxide layer after isothermal exposure for 30 min, μm			Thickness of the oxide layer after isothermal exposure for 5 h, μm				
	surface / Mg saturated	sublayer (based on ZrO_2)	h_{Σ}	surface / Mg saturated	sublayer			h_{Σ}
					based on SiO_2	based on ZrO_2	based on SiO_2	
1	5-7 / 3-5	220-230	225-240	4-6 / 4-6	90-100	160-170	260-270	515-535
2	5-7 / 3-5	155-170	160-180	18-20 / 4-6	–	170-180	150-160	340-360
3	12-17 / 9-12	320-340	335-355	15-20 / 15-20	130-140	390-410	–	550-570

A distinctive feature of experiments on the oxidation of HP samples of the $ZrSi_2$-$MoSi_2$-ZrB_2 system with isothermal exposure at a temperature of 1650°C is the presence of low-temperature stages associated with heating and cooling of compacts with a furnace. Therefore, the results obtained integrally reflect the behavior of samples during thermal cycling in the range of 20-1650°C, including conditions (~ 750-1250°C), when the protective properties of oxide films cannot be fully realized.

It is assumed that the dominant chemical process is the oxidation of $ZrSi_2$ by reaction (1). The melting of $ZrSi_2$ in the peritectic reaction, starting at a temperature of 1620°C, causes the appearance of a liquid silicon phase. The liquid phase provides faster mass transfer of reagents [2, 9], which additionally accelerates the oxidation process. Also, the oxidation of $MoSi_2$, ZrB_2 phases takes place according to reactions (2), (3) and the formation of borosilicate glass by reaction (4). The calculated values of the isobaric-isothermal potential ΔG at 1650°C for reactions (1) - (4) are, respectively, kJ/mol: -1733.2; -3714.7; -2562.8; < 0 (specific value depends on the ratio of the coefficients x and y).

The formation of the zircon phase by reaction (5) according to thermodynamic calculations is possible at temperatures of up to ~ 1539°C, at which ΔG changes its sign from negative to positive. With increasing temperature, reaction (5) goes in the opposite direction, i.e. thermal dissociation of $ZrSiO_4$ to the initial oxide components SiO_2 and ZrO_2 is observed. The results of the structural-phase studies performed by us on the $ZrSi_2$-$MoSi_2$-ZrB_2 system after oxidation showed that the proportion of the $ZrSiO_4$ phase in the structure of the oxide layers is low. At the same time, the detected particles are surrounded by SiO_2 silica. It is probably that the presence of an external SiO_2 shell enveloping the $ZrSiO_4$ phase shifts the chemical equilibrium of reaction (5) towards the formation of the final product, i.e. raises the dissociation temperature of $ZrSiO_4$.

In the process of oxidation and dissociation, a multilayer oxide film is formed, which is represented by (i) a surface layer of silicate glass with separately located $ZrSiO_4$ particles (ii) ZrO_2 and SiO_2 based sublayers. A part of silicon dioxide SiO_2, formed during the oxidation of $ZrSi_2$, $MoSi_2$ and dissociation of $ZrSiO_4$, remains in the bulk of the oxide film and fills the pores that are not occupied by ZrO_2. The other part is transferred to the surface, ensuring the formation of a continuous vitreous layer. Upwelling, as well as at 1400°C, is driven by volume expansion during oxidation. The formation of borosilicate glass according to reaction (4) reduces the viscosity of the melt and facilitates its

transport to the surface. At the same time, magnesium is segregated in the outer part of the outer oxide layer in the same way as described in section 3.2. It should be noted that the observed thickness of the surface glass layer after oxidation at 1650°C seems to be thinner than the thickness of the layer formed at less high temperatures, due to possible partial evaporation of the silicate glass.

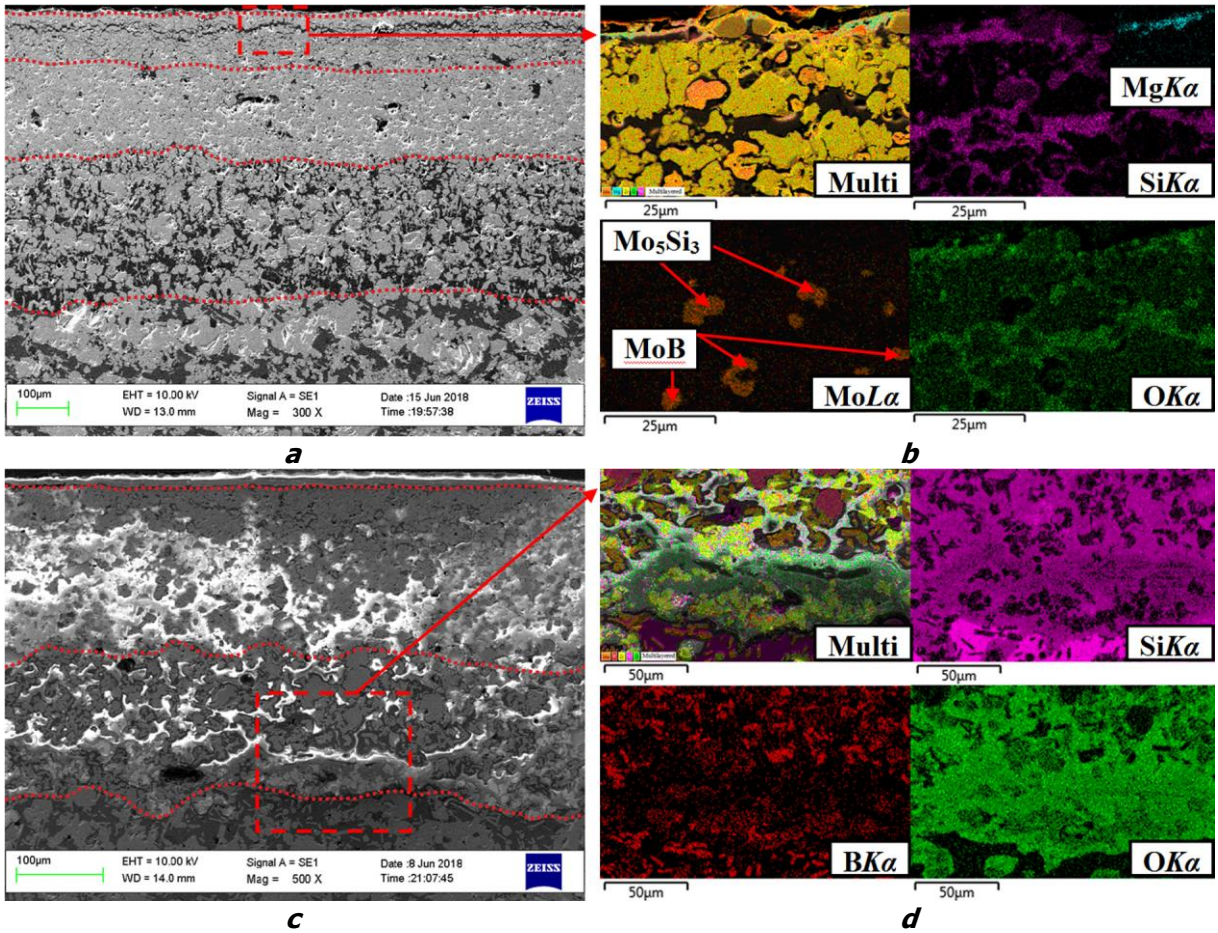

Fig. 4. Microstructure (*a*, *c*) and distribution of elements in characteristic X-rays (*b*, *d*) in samples after isothermal oxidation at 1650°C, 5 hours: composition *1* - *a*, *b*; composition *2* - *c*, *d*

A characteristic feature of the oxidation of compositions *1* and *2* at 1650°C is the formation in the upper part of their subsurface oxide layer of the secondary phases Mo_5Si_3 and MoB according to reactions (2) and (6), where B_2O_3 in (6) is the oxidation product of ZrB_2 by reaction (3):

$$4MoSi_{2(s)} + 2B_2O_{3(l)} + 5O_{2(g)} \rightarrow 8SiO_{2(s)} + 4MoB_{(s)} \ (\Delta G_{1650°C} = -2828.2 \text{ kJ/mol}). \quad (6)$$

The decrease in the partial pressure of oxygen over the thickness of the oxide film together with the encapsulation of ZrB_2 particles in the silicate matrix explains the impossibility of carrying out the reaction (6) in the deep oxide layers. The resulting Mo_5Si_3 and MoB phases are highly heat-resistant [9] and refractory (their melting points are 2180 and 2600°C, respectively). Interestingly, after oxidation of ceramics of composition $85ZrB_2$-$15MoSi_2$ (vol. %) At 1650°C for 15 min, the authors of [9] found the presence of an interlayer in the oxide zone consisting of MoB particles tightly adjacent to each other. According to the results of our studies, after oxidation of ceramics of the $ZrSi_2$-$MoSi_2$-ZrB_2 system at 20-1650°C with an exposure at a maximum temperature of 5 hours, the MoB segregations is represented by individual particles located at a considerable distance from each other. These differences should be attributed to the dominant role of the liquid-phase oxidation of $ZrSi_2$, as a result of which the resulting glass phase envelops the ZrB_2 and $MoSi_2$ particles, limiting the access of oxygen required for reactions (3) and (6). The absence of MoB particles in the oxide zone of composition *3* is obviously due to the high degree of distribution of the glass phase between the structural components, which leads to a more complete encapsulation of ZrB_2 and $MoSi_2$ particles.

The coefficients in the regression equations are calculated by the Levenberg-Marquardt algorithm using the least squares method. The calculations were performed in a mathematical package of the

MathCAD software product. Analysis of the constructed response surfaces in the form of diagrams "phase composition - heat resistance" made it possible to establish that an increase in the content of ZrB_2 and $MoSi_2$ phases in the structure of ceramics leads to an increase in their heat resistance at 1650°C, and the $ZrSi_2$ phase together with $ZrSiO_4$ - on the contrary, to decrease (Fig. 5).

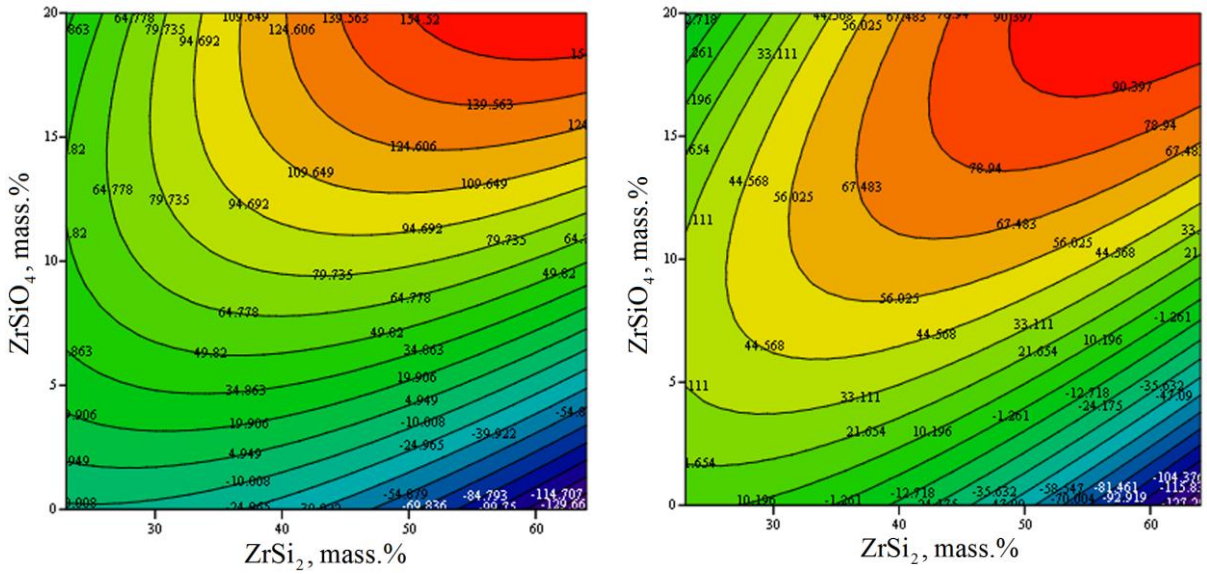

Fig. 5. Calculated diagram "phase composition - heat resistance" for ceramics of $ZrSi_2$-$MoSi_2$-ZrB_2 system at 1650°C: $MoSi_2$ = 7 mass. % (*a*), $MoSi_2$ = 17 mass. % (*b*)

A physicochemical interaction in the $ZrSi_2$-$ZrSiO_4$ system, not previously described in the literature, was found, resulting in the reduction of elemental silicon with simultaneous oxidation of zirconium to a thermodynamically stable ZrO_2 phase. In conditions of lack or absence of oxygen, the interaction at temperatures above 1620°C is described by the following equation (7):

$$ZrSi_{2(l)} + ZrSiO_{4(s)} = 2ZrO_{2(s)} + 3Si_{(l)}. \quad (7)$$

The reaction proceeds with an increase in the volume of products, which leads to an increase in the internal pressure in the samples, under the action of which (together with capillary forces) silicon and/or eutectics (Si + $ZrSi_2$) exit to the outside. This explains the appearance of blisters, fistulas and sweating droplets on the surface of the samples.

4. Conclusions

1. Ceramic materials in the $ZrSi_2$-$MoSi_2$-ZrB_2 system were produced by a combination of SHS technologies and hot pressing.

2. The kinetics and mechanism of high-temperature oxidation of ceramics was studied at temperatures of 1400 and 1650°C for 10 and 5 hours, respectively. The influence of the $ZrSi_2$, $MoSi_2$ and ZrB_2 phases on the structural-morphological features of the formation of oxide films and the effectiveness of their protective action was analyzed.

3. During oxidation at 1400°C, a two-layer structure is formed. It consists of a continuous silicate film, the outer part of which is saturated with magnesium, and a sublayer based on the $ZrSiO_4$ phase with a scheelite structure encapsulating ZrB_2 and $MoSi_2$ grains.

4. During oxidation at 1650°C, a multilayer structure is formed. It consists of a layer of complex silicate glass and sublayers based on ZrO_2 and SiO_2. Partial dissociation of $ZrSiO_4$ and the formation of MoB and Mo_5Si_3 secondary phases are noted. Above 1620°C under conditions of oxygen deficiency in the $ZrSi_2$-$ZrSiO_4$ system, the reduction of silicon with simultaneous oxidation of zirconium to the thermodynamically stable ZrO_2 phase was established.

Acknowledgements

The study was supported by the Ministry of Education and Science of the Russian Federation within the framework of state assignment (No. 9.1077.2017/PCH).

References

1. *Johnson, S.M.* Ultra high temperature ceramics (UHTCs) // *Proceedings of the Thermal protection system technical interchange meeting (TPS TIM)*. Langley research center, Moffett field, California, USA, September 29-30, 2015. Pp. 1–65. https://ntrs.nasa.gov/archive/nasa/casi.ntrs.nasa.gov/20150022996.pdf
2. *Astapov, A.N., Terent'eva, V.S.* Review of domestic designs in the field of protecting carbonaceous materials against gas corrosion and erosion in high-speed plasma fluxes // *Russian Journal of Non-Ferrous Metals*. 2016. Vol. 57. No. 2. Pp. 157–173. DOI: 10.3103/S1067821216020048.
3. *Jin, X., Fan, X., Lu, C., Wang, T.* Advances in oxidation and ablation resistance of high and ultra-high temperature ceramics modified or coated carbon/carbon composites // *Journal of the European Ceramic Society*. 2018. Vol. 38. No. 1. Pp. 1–28. DOI: 10.1016/j.jeurceramsoc.2017.08.013.
4. *Yurishcheva, A.A., Astapov, A.N., Lifanov, I.P., Rabinskiy, L.N.* High temperature coatings for oxidation and erosion protection of heat-resistant carbonaceous materials in high-speed flows // *Key Engineering Materials*. 2018. Vol. 771. Pp. 103–117. DOI: 10.4028/www.scientific.net/KEM.771.103.
5. *Grigoriev, O.N., Galanov, B.A., Lavrenko, V.A., Panasyuk, A.D., Ivanov, S.M., Koroteev, A.V., Nickel, K.G.* Oxidation of ZrB_2-SiC-$ZrSi_2$ ceramics in oxygen // *Journal of the European Ceramic Society*. 2010. Vol. 30. No. 11. Pp. 2397–2405. DOI: 10.1016/j.jeurceramsoc.2010.03.016.
6. *Lavrenko, V.O., Panasyuk, A.D., Grigorev, O.M., Koroteev, O.V., Kotenko, V.A.* High-temperature oxidation of ZrB_2-SiC and ZrB_2-SiC-$ZrSi_2$ ceramics up to 1700 °C in air // *Powder Metallurgy and Metal Ceramics*. 2012. Vol. 51. No 3–4. Pp. 217–221. DOI: 10.1007/s11106-012-9420-7.
7. *Sciti, D., Silvestroni, L., Saccone, G., Alfano, D.* Effect of different sintering aids on thermo-mechanical properties and oxidation of SiC fibers – Reinforced ZrB_2 composites // *Materials Chemistry and Physics*. 2013. Vol. 137. No. 3. Pp. 834–842. DOI: 10.1016/j.matchemphys.2012.09.071.
8. *Qi, Li, Lamei, Cao, Xiaosu, Yi*. Oxidation behavior of a SPS sintered ZrB_2-SiC-$MoSi_2$ ceramic at 1500 °C // *MATEC Web of Conferences*. 2016. Vol. 67. No. UNSP 06079. Pp. 1–9. DOI: 10.1051/matecconf/20166706079.
9. *Silvestroni, L., Meriggi, G., Sciti, D.* Oxidation behavior of ZrB_2 composites doped with various transition metal silicides // *Corrosion Science*. 2014. Vol. 83. Pp. 281–291. DOI: 10.1016/j.corsci.2014.02.026.
10. *Lavrenko, V.O., Panasyuk, A.D., Grigorev, O.M., Koroteev, O.V., Kotenko, V.A.* High-temperature (to 1600 °C) oxidation of ZrB_2-$MoSi_2$ ceramics in air // *Powder Metallurgy and Metal Ceramics*. 2012. Vol. 51. No 1–2. Pp. 102–107. DOI: 10.1007/s11106-012-9403-8.
11. *Sciti, D., Brach, M., Bellosi, A.* Oxidation behavior of a pressureless sintered ZrB_2-$MoSi_2$ ceramic composite // *Journal of Materials Research.* 2005. Vol. 20. No. 4. Pp. 922–930. DOI: 10.1557/JMR.2005.0111.
12. *Yatsyuk, I.V., Pogozhev, Yu.S., Levashov, E.A., Novikov, A.V., Kochetov, N.A., Kovalev, D.Yu.* Features of production and high-temperature oxidation of SHS ceramics based on zirconium boride and zirconium silicide // *Izvestiya Vuzov. Poroshkovaya Metallurgiya i Funktsional'nye Pokrytiya.* 2017. No. 1. Pp. 29–41. DOI: 10.17073/1997-308X-2017-1-29-41. (In Russian).
13. *Levashov, E.A., Rogachev, A.S., Kurbatkina, V.V., Maksimov, Yu.M., Yukhvid, V.I.* Promising materials and technologies of self-propagating high-temperature synthesis. – Moscow: Izd. Dom MISiS, 2011. 377 p. (In Russian).
14. *Ratnikov, V.I., Borovinskaya, I.P., Prokudina, V.K*. The pilot equipment for SHS. Safety and standardization // *Izvestiya Vuzov. Poroshkovaya Metallurgiya i Funktsional'nye Pokrytiya. 2013.* No. 1. PP. 34–41. DOI: 10.17073/1997-308X-2013-1-34-41. (In Russian).